

MODELING THE SYSTEM PARAMETERS OF 2M 1533+3759: A NEW LONGER PERIOD LOW-MASS ECLIPSING sdB+dM BINARY

B.-Q. FOR¹, E. M. GREEN², G. FONTAINE³, H. DRECHSEL⁴, J. S. SHAW⁵, J. A. DITTMANN², A. G. FAY², M. FRANCOEUR³, J. LAIRD², E. MORIYAMA², M. MORRIS², C. RODRÍGUEZ-LÓPEZ⁶, J. M. SIERCHIO², S. M. STORY², A. STROM², C. WANG², S. M. ADAMS², D. E. BOLIN², M. ESKEW², AND P. CHAYER⁷

¹ Department of Astronomy, University of Texas, Austin, TX 78712, USA; bjqing@astro.as.utexas.edu

² Steward Observatory, University of Arizona, 933 North Cherry Avenue, Tucson, AZ 85721, USA

³ Département de Physique, Université de Montréal, Montréal, QC H3C 3J7, Canada

⁴ Dr. Remeis-Sternwarte Bamberg, Astronomisches Institut der Universität Erlangen-Nürnberg, Sternwartstraße 7, 96049, Germany

⁵ Department of Physics and Astronomy, University of Georgia, Athens, GA 30602, USA

⁶ Laboratoire d’Astrophysique de Toulouse-Tarbes, Université de Toulouse, CNRS, 14 Av. Edouard Belin, Toulouse 31400, France

⁷ Space Telescope Science Institute, 3700 San Martin Drive, Baltimore, MD 21218, USA

Received 2009 July 21; accepted 2009 November 6; published 2009 December 10

ABSTRACT

We present new photometric and spectroscopic observations for 2M 1533+3759 (= NSVS 07826147), the seventh eclipsing subdwarf B star + M dwarf (sdB+dM) binary ever found. It has an orbital period of 0.16177042 days, or ~ 3.88 hr, significantly longer than the 2.3–3.0 hr periods of the other known eclipsing sdB+dM systems. Spectroscopic analysis of the hot primary yields $T_{\text{eff}} = 29230 \pm 125$ K, $\log g = 5.58 \pm 0.03$, and $\log N(\text{He})/N(\text{H}) = -2.37 \pm 0.05$. The sdB velocity amplitude is $K_1 = 71.1 \pm 1.0$ km s⁻¹. The only detectable light contribution from the secondary is due to the surprisingly strong reflection effect, whose peak-to-peak *BVR*I amplitudes are 0.10, 0.13, 0.15, and 0.19 mag, respectively. Light-curve modeling produced several solutions corresponding to different values of the system mass ratio, q (M_2/M_1), but only one is consistent with a core helium burning star, $q = 0.301$. The orbital inclination is 86°.6. The sdB primary mass is $M_1 = 0.376 \pm 0.055 M_{\odot}$ and its radius is $R_1 = 0.166 \pm 0.007 R_{\odot}$. 2M 1533+3759 joins PG 0911+456 (and possibly also HS 2333+3927) in having an unusually low mass for an sdB star. sdB stars with masses significantly lower than the canonical value of $0.48 M_{\odot}$, down to as low as $0.30 M_{\odot}$, were theoretically predicted by Han et al., but observational evidence has only recently begun to confirm the existence of such stars. The existence of core helium burning stars with masses lower than 0.40 – $0.43 M_{\odot}$ implies that at least some sdB progenitors have initial main-sequence masses of 1.8 – $2.0 M_{\odot}$ or more, i.e., they are at least main-sequence A stars. The orbital separation in 2M 1533+3759 is $a = 0.98 \pm 0.04 R_{\odot}$. The secondary has $M_2 = 0.113 \pm 0.017 M_{\odot}$, $R_2 = 0.152 \pm 0.005 R_{\odot}$, and $T_{\text{eff}2} = 3100 \pm 600$ K, consistent with a main-sequence M5 star. If 2M 1533+3759 becomes a cataclysmic variable (CV), its orbital period will be 1.6 hr, below the CV period gap.

Key words: binaries: eclipsing – stars: fundamental parameters – stars: individual (2M 1533+3759) – subdwarfs

1. INTRODUCTION

Subdwarf B (sdB) stars are evolved, hot, compact stars ($23,000 \text{ K} < T_{\text{eff}} < 37,000 \text{ K}$; $5.2 < \log g < 6.0$), commonly found in the disk and halo of our Galaxy (Saffer et al. 1994). They are believed to ascend the first red giant branch (RGB) following the exhaustion of central hydrogen, somehow experiencing sufficient mass loss prior to the RGB tip to remove nearly all of their envelopes. They subsequently evolve blueward from the RGB before igniting helium in their cores. From an evolutionary point of view, sdB stars are also known as extreme horizontal branch stars (Heber 1986). Their helium burning cores, generally expected to be just under $0.5 M_{\odot}$, are essentially identical to those of normal horizontal branch stars. However, their hydrogen envelopes are too thin and inert ($< 0.01 M_{\odot}$) (Saffer et al. 1994; Heber 1986) to support double shell burning, so they never make it to the asymptotic giant branch. Following core helium exhaustion, they evolve directly into sdO stars before proceeding down the white dwarf cooling track (Dorman et al. 1993).

In the context of understanding Galaxy evolution and cosmology, sdB stars play an important role because their large UV flux appears to be the dominant source of the “UV upturn” phenomenon observed in elliptical galaxies and the centers of

spiral bulges (de Boer 1982; Greggio & Renzini 1999; Brown et al. 1997). The UV excess in old stellar populations has been used as an age indicator in evolutionary population synthesis (Yi et al. 1997, 1999), although more recent work has begun to consider alternative binary scenarios that would have quite different effects (Podsiadlowski et al. 2008).

Various evolutionary scenarios have been proposed for sdB stars, but the details of the formation mechanisms are not yet well determined. Possible formation channels can be divided into single star evolution with enhanced mass loss at the tip of RGB (Castellani & Castellani 1993; D’Cruz et al. 1996) and close binary evolution, first suggested by Mengel et al. (1976). Recently, Han et al. (2002, 2003) conducted an in-depth theoretical investigation through binary population synthesis. They found that common-envelope evolution, resulting from dynamically unstable mass transfer near the tip of the first RGB, should produce short-period binaries ($P \approx 0.1$ – 10 days) with either a main-sequence (MS) or white dwarf (WD) companion. If a red giant star loses nearly all of its envelope prior to the red giant tip via stable mass transfer, a long-period sdB binary with an MS companion can be produced ($P \approx 10$ – 500 days). A most interesting feature of Han et al.’s models is that they predict a much larger range of sdB progenitor masses than had previously been considered, including stars sufficiently massive to avoid a

Table 1
sdB Stars with Masses Determined by Asteroseismology

Name	$\log g$ (cm s^{-2})	T_{eff} (K)	M_1 (M_{\odot})	$\log M_{\text{env}}/M_{*}$	References
PG 1047+003	5.800 ± 0.006	33150 ± 200	0.490 ± 0.014	-3.72 ± 0.11	Charpinet et al. (2003)
PG 0014+067	5.775 ± 0.009	34130 ± 370	0.477 ± 0.024	-4.32 ± 0.23	Charpinet et al. (2005a)
PG 1219+534	5.807 ± 0.006	33600 ± 370	0.457 ± 0.012	-4.25 ± 0.15	Charpinet et al. (2005b)
PG 1325+101	5.811 ± 0.004	35050 ± 220	0.499 ± 0.011	-4.18 ± 0.10	Charpinet et al. (2006)
EC 20117–4014	5.856 ± 0.008	34800 ± 2000	0.540 ± 0.040	-4.17 ± 0.08	Randall et al. (2006)
PG 0911+456	5.777 ± 0.002	31940 ± 220	0.390 ± 0.010	-4.69 ± 0.07	Randall et al. (2007)
Feige 48	5.462 ± 0.006	29580 ± 370	0.519 ± 0.009	-2.52 ± 0.06	van Grootel et al. (2008a)
BAL 090100001	5.383 ± 0.004	28000 ± 1200	0.432 ± 0.015	-4.89 ± 0.14	van Grootel et al. (2008b)
PG 1336–018	5.739 ± 0.002	32740 ± 400	0.459 ± 0.005	-4.54 ± 0.07	Charpinet et al. (2008)
PG 1605 + 072	5.226 ± 0.005	32300 ± 400	0.528 ± 0.004	-5.88 ± 0.04	van Spaandonk et al. (2008)
EC 09582–1137	5.788 ± 0.004	34805 ± 230	0.485 ± 0.011	-4.39 ± 0.10	Randall et al. (2009)

helium flash and instead undergo quiescent helium ignition in non-degenerate cores (see also Hu et al. 2007; Politano et al. 2008).

Binary formation scenarios appear likely to be responsible for the majority of observed field sdB stars, as a large fraction are observed to occur in binaries (e.g., Lisker et al. 2005; Morales-Rueda et al. 2003; Maxted et al. 2001; Saffer et al. 2001; Green et al. 1997; Allard et al. 1994). Nevertheless, the same studies show that there are a sizable fraction of sdB stars, 30% or more, that do not now appear to be in binaries: there is no sign of a companion in high S/N optical spectra or infrared colors, and their radial velocities are constant to within the observational errors (a few km s^{-1}) over many months. Moni Bidin et al. (2008) also found a significant fraction, 96%, of sdB stars in globular clusters to be single stars, in contrast to observed field sdB stars. Han et al. (2002, 2003) investigated the possibility of forming single sdB stars by merging two helium white dwarfs, which would allow the formation of more massive sdB stars ($0.4\text{--}0.65 M_{\odot}$), and Politano et al. (2008) considered the possibility that some sdB stars might form from mergers during common envelope evolution, followed by rotationally induced mass loss. Still, unusually high mass loss in single red giant stars cannot yet be ruled out.

The distribution of sdB masses is clearly one of the most important constraints on the several possible formation channels. Different observational techniques provide different windows of opportunity for investigating these masses.

More sdB masses have been derived by asteroseismology than by any other method to date. Asteroseismology provides an extremely high level of precision (and is the only way to determine envelope masses, in addition to total masses), but it has so far been successfully applied only to the relatively rare short-period sdB pulsators. Two different types of multimode sdB pulsators have been discovered: short-period V361 Hya pulsators (originally, EC 14026 stars; Kilkeny et al. 1997) which comprise a rather small percentage of the hotter sdB stars, and longer period V1093 Her pulsators (PG 1716 stars; Green et al. 2003), which seem to be fairly common among cooler sdB stars. The rapid oscillations of V361 Hya stars are interpreted as low-order pressure modes (p -modes) that are driven by a κ -mechanism associated with the radiative levitation of iron in the thin diffusion-dominated envelopes (Charpinet et al. 1996, 1997). The same mechanism has also been shown to explain the excitation of high-order gravity modes (g -modes) in the V1093 Her stars (Fontaine et al. 2003). Asteroseismological modeling has so far been extremely successful with p -mode pulsations in the envelopes of sdB stars, and the resulting

stellar parameters are generally in very good agreement with theoretical expectations (e.g., Fontaine et al. 2008; Charpinet et al. 2007, and references therein). On the other hand, g -mode pulsations, which extend much more deeply into the stellar cores, will require more sophisticated interior models before they can be satisfactorily analyzed by asteroseismology (Randall et al. 2007).

The list of p -mode pulsators whose parameters have been derived by asteroseismology is presented in Table 1. Most of the derived masses are within a few hundredths of a solar mass of the canonical sdB mass of $0.48 M_{\odot}$, except for PG 0911+456 (Randall et al. 2007), which will be discussed further in Section 7. Interestingly, the only post-common envelope binaries in this list are Feige 48 (van Grootel et al. 2008a) and PG 1336–018 (Charpinet et al. 2008). Indeed, the large majority of V1093 Her stars exhibit low or negligible radial velocity variations, of the order of a few km s^{-1} or less, and thus must be single stars, or have extremely low-mass companions, or else occur in long-period binaries with a main-sequence F, G, or K star primary. This is not surprising, since sdB stars whose radial velocity variations are clearly indicative of post-common envelope binaries are preferentially found at temperatures cooler than most V1093 Her stars (Green et al. 2008).

Traditional methods of deriving masses by exploiting binary properties are therefore quite important. For one thing, binaries provide a vital test of asteroseismology in the rare cases where the sdB primary is a pulsator. More importantly, until improved asteroseismic models and extensive satellite observations make it possible to successfully model g -mode sdB pulsators, the only way to derive masses for a larger sample of post-common envelope sdB stars is to analyze their binary properties. Finally, there are simply a large number of binaries that contain non-pulsating sdB stars.

The difficulty with most sdB stars in post-common envelope systems is that they are single-lined spectroscopic binaries with essentially invisible compact secondaries. In principle, precise measurements of the sdB surface gravity and rotational velocity in a tidally locked system will yield the orbital inclination, allowing the individual component masses to be determined from the mass function (e.g., Geier et al. 2008), but the accuracy of this approach has not yet been proven. There are, however, a small number of rare post-common envelope sdB+dM binaries (Maxted et al. 2004), which have been identified by their reflection effects—e.g., the sinusoidal variation observed in the light curve due to reradiated light from the heated side of the tidally locked M dwarf—that are more promising. The known sdB+dM systems are summarized in Table 2. If narrow lines

Table 2
Currently Known sdB+dM Binaries

Name	Alternate Name	Period (day)	M_1 (M_\odot)	M_2 (M_\odot)	References	Comments
Reflection Effect/Eclipsing Binaries						
HS 0705+6700		0.0956466	0.48	0.13	Drechsel et al. (2001)	Light curve
PG 1336–018	NY Vir	0.101015999	0.466/0.389	0.122/0.110	Vučković et al. (2007)	Light curve, two solutions
NSVS 14256825	J 2020+0437	0.1104	0.459	...	Charpinet et al. (2008)	Asteroseismology
HS 2231+2441		0.11058798	0.46	0.21	Wils et al. (2007)	No spectroscopy
PG 1241–084	HW Vir	0.11676195	< 0.3	...	Østensen et al. (2008)	Uncertain log g
BUL–SC16 335		0.125050278	0.485	0.142	Lee et al. (2009)	Light curve
2M 1533+3759	NSVS 07826147	0.16177042	Polubek et al. (2007)	
			0.377	0.113	this paper	Light curve
Reflection Effect/Non-eclipsing Binaries						
PG 1017–086	XY Sex	0.073	Maxted et al. (2002)	
HS 2333+3927		0.1718023	0.38	0.29	Heber et al. (2005)	Light curve
PG 1329+159	Feige 81, PB 3963	0.249699	Maxted et al. (2004)	
		0.249702	Green et al. (2004)	
2M 1926+3720	KBS 13	0.2923	For et al. (2008)	
PG 1438–029		0.33579	Green et al. (2004)	
HE 0230–4323		0.4515	Koen (2007)	

originating from the cool secondary could be detected, then masses of both components could be derived from the double-lined spectroscopic solution. Again, this should be possible, in principle, especially in binaries with the shortest orbital periods, where the heated face of the secondary is brighter than it otherwise would be, but results so far have been ambiguous. Vučković et al. (2008) detected emission lines from the secondary in PG 1336–018 by subtracting the spectrum of the hot primary from spectra taken at other phases, but the S/N of the spectra was only sufficient to claim general consistency with the orbital solution described in Vučković et al. (2007). Using much higher S/N spectra of a similar sdO+dM binary, AA Dor, Vučković et al. (2008) were able to determine a velocity amplitude for the secondary, but their derived primary mass has now been vigorously disputed by Rucinski (2009). Wood & Saffer (1999) presented a good argument for the detection of H α absorption lines from the secondary in HW Vir, again by subtracting the spectrum near minimum light from spectra near maximum light, and obtained reasonable velocities, but it is perplexing that absorption lines and no emission lines should have been seen.

An apparently more successful method is to model the light variations in sdB+dM binaries exhibiting reflection effects, especially the eclipsing systems, in order to determine the system parameters. This is a very complex endeavor. The models have many free parameters, and there are large uncertainties that typically require additional information to constrain the solution. Often, the light curves provide more than one high-quality solution. For example, Drechsel et al. (2001) had to make use of a mass–radius relation for the secondary star to decide between two solutions that implied quite different sdB masses for HS 0705+6700 (0.483 and <0.3 M_\odot). Heber et al. (2004) needed to use their spectroscopic log g and mass–radius relations to discriminate between two solutions with different secondary albedos and inclinations in HS 2333+3927. Vučković et al. (2007) found three possible solutions modeling the light curves PG 1336–018, and it was not possible to choose between two of them until Charpinet et al. (2008) derived a consistent primary mass by asteroseismological modeling. Furthermore, even when a single family of solutions can be identified, there

still remain unavoidable ambiguities in choosing one “best” model (Drechsel et al. 2001). Even in the most favorable cases of eclipsing sdB+dM binaries, the eclipses are not flat-bottomed, leading to a small range of nearly equivalent solutions in the vicinity of the deepest minimum. The resulting small variations in the mass ratio, q , lead to a significant range in the derived sdB mass. The uncertainties are obviously larger when there is no eclipse. Still, light-curve modeling provides valuable information, and when the derived sdB mass can be verified—rarely by asteroseismology, more often from consistency with the spectroscopic surface gravity or projected rotational velocity—our confidence in the results is greatly increased. It is clearly important to investigate as many sdB+dM binaries as possible, especially the eclipsing systems, in order to build up a more comprehensive picture of sdB masses produced by post-common envelope evolution and to compare with the distribution of masses from other formation channels.

In this paper, we report on the system parameters of 2M 1533+3759 (15^h33^m49^s.44, +37°59′28″.2, J2000), a new eclipsing sdB+dM binary with a longer orbital period than any eclipsing sdB+dM discovered so far. This star was first recognized as an sdB in 2005 (although it remained unpublished) during a continuing spectroscopic survey (Green et al. 2008) of bright blue stellar candidates selected from a variety of sources, including the 2MASS survey (Skrutskie et al. 2006). The current investigation was motivated by Kelley & Shaw (2007), who discovered that 2M 1533+3759 is an eclipsing binary, NSVS 07826147, through their work with the Northern Sky Variability Survey (NSVS; Wozniak et al. 2004). Kelley & Shaw (2007) identified a group of nine eclipsing binaries with short periods and relatively narrow eclipse widths, indicating very small radii for the components. Since their list includes the well-known HW Vir (Lee et al. 2009 and references therein), as well as 2M 1533+3759, which we confirmed to be a spectroscopic near-twin of HW Vir, Kelley & Shaw (2007) proposed that the other objects in their Table 3 might also be sdB+dM binaries. Section 2 presents the results from our follow-up spectra for these stars.

In Section 3, we describe new spectroscopy and photometry for 2M 1533+3759. The data analyses are given in Sections 4

Table 3
NSVS Sources Identified by Kelley & Shaw (2007) as Potential sdB Stars

NSVS ID ^a	V^a (mag)	Period ^a (day)	$J - H^b$ (mag)	R.A. (J2000) ^b (h m s)	Decl. (J2000) ^b ($^{\circ}$ $'$ $''$)	Spectral Type ^c	Comments
02335765	10.69	9.744983	0.224	06:31:02.7	+61:14:29	F2–F5	
03259747	11.22	1.239805	0.274	20:57:27.7	+56:46:06	F9–G0	
04818255	12.10	0.1600359	0.392	08:40:58.4	+39:56:28	G0	Late-type eclipsing binary star
			0.343	08:41:00.2	+39:55:54	F9–G0	Star nearest to NSVS coords
04963674	10.63	3.6390769	0.297	11:03:36.4	+41:36:02	F9–G0	
07826147	13.61	0.16177	−0.084	15:33:49.4	+37:59:28	sdB	2M 1533+3759; FBS 1531+381
08086052	11.94	1.853631	0.255	18:03:11.9	+32:11:14	F8–F9	
09729507	11.77	4.740887	0.094	06:05:18.4	+20:44:32	A0–A2	
15864165	12.65	1.232349	0.111	11:05:06.6	−09:01:33	A6–A7	
15972828	11.21	0.116719	−0.119	12:44:20.2	−08:40:16	sdB	HW Vir

Notes.

^a Table 3 of Kelley & Shaw (2007)

^b 2MASS Point Source Catalog (Skrutskie et al. 2006)

^c Steward 2.3 m spectra

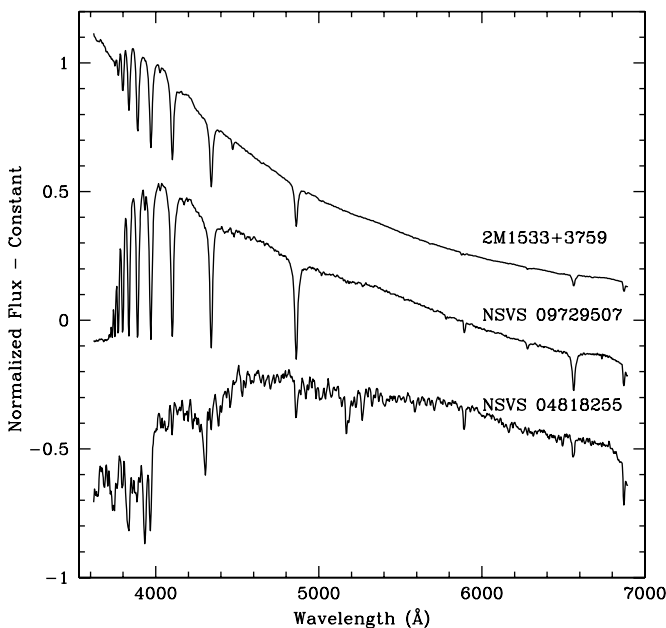


Figure 1. Flux-calibrated 2M 1533+3759 spectrum compared to the bluest and reddest non-sdB spectra from Table 3.

and 5, and the system parameters are derived in Section 6. We discuss possible selection effects and consider the unusually low derived mass for the sdB mass in Section 7. Section 8 looks at the evolution of 2M 1533+3759, and Section 9 contains our conclusions.

2. NSVS ECLIPSING SDB+DM CANDIDATES

We have obtained high S/N low-resolution spectra for Kelley & Shaw’s (2007) proposed sdB+dM stars (their Table 3). All were observed with the same telescope and instrumental setup (Section 3) that we used to obtain our initial spectrum of 2M 1533+3759.

Table 3 of this paper presents the results of our spectroscopic follow-up. The NSVS numbers, V magnitudes, and orbital periods from Kelley & Shaw are listed in the first three columns. Columns 4, 5, and 6 give the $J - H$ color, R.A., and decl. from the Two Micron All-Sky (2MASS) Point Source Catalog (Skrutskie

et al. 2006) for the objects that we observed. The seventh column lists our best estimate of their spectral types. For the non-sdB stars, the spectral types were determined by cross-correlating their continuum-subtracted spectra with template spectra of known main-sequence spectral standards (Gray & Corbally 2009), acquired with the same instrument and spectroscopic setup, in order to find the best match. Since the binary spectra are composite, the best matches indicate either the dominant or the effective spectral type.

NSVS 04818255 deserves further comment. Its NSVS coordinates are $08^{\text{h}}40^{\text{m}}59^{\text{s}}.8$, $+39^{\circ}56'02''$; this is close, but not quite coincident with the brightest star in the immediate area. Kelley & Shaw identified NSVS 04818255 with the sdB star PG 0837+401. However, according to the finder chart in Green et al. (1986), PG 0837+401 is the fainter star at $08^{\text{h}}41^{\text{m}}01^{\text{s}}.3$, $+39^{\circ}56'18''$, approximately $24''$ northeast; our spectrum confirms that it is indeed an sdB star. We initially observed the bright F9–G0 star nearest to the NSVS coordinates, since it has the same 2MASS $J - H$ value that Kelley & Shaw give for NSVS 04818255. However, S. Bloemen and I. Decoster (Leuven) and M. Godart (Liège) recently obtained timeseries photometry indicating that neither PG 0837+401 nor the bright F9–G0 star are variable (R. Østensen 2009, private communication). The eclipsing system that they identify with NSVS 04818255 is the intermediate brightness object almost $40''$ west northwest of PG 0837+401. We obtained a spectrum for the variable star and found it to have a G0 spectral type, in agreement with its somewhat redder $J - H$.

HW Vir and 2M 1533+3759 are therefore, unfortunately, the only two bona fide sdB stars in Kelley & Shaw’s (2007) list. Figure 1 shows our flux-calibrated spectrum for 2M 1533+3759, along with the bluest and reddest of the non-sdB spectra from Table 3, for comparison. It is clear from the decreasing flux blueward of the Balmer jump that there are not any sdB stars hidden in any of the seven binaries with overall A, F, or G spectral types. $J - H$ colors are a good indicator for the presence of an sdB star in a suspected sdB+dM binary, since M dwarfs later than about M2 are too faint relative to sdB stars to have much of an effect on the $J - H$ colors. All of the known sdB+dM binaries have $-0.2 < J - H < 0.0$; their distribution in $J - H$ is only slightly redder than the overall distribution of moderately unreddened sdB+WD binaries and non-binary sdB stars plotted in Green et al.’s (2008) Figure 5.

Table 4
Low Resolution 2.3 m Spectra

UT Date	HJD at Midpoint (2450000+)	Exp Time (s)	S/N	Orbital Phase
2005 Jun 27	3548.82037	550	165	0.72
2007 Dec 30	4465.04391	480	174	0.44
2007 Dec 31	4466.03402	400	161	0.56
2008 Jan 19	4485.02730	490	162	0.97
2008 Sep 19	4728.61983	450	179	0.76

3. OBSERVATIONS AND REDUCTIONS

3.1. Spectroscopy

Low-resolution spectra for 2M 1533+3759 were obtained with the Boller & Chivens (B&C) Cassegrain spectrograph at Steward Observatory's 2.3 m Bok telescope on Kitt Peak. The 400 mm^{-1} first-order grating was used with a $2''.5$ slit to obtain spectra with a typical resolution of 9 \AA over the wavelength interval $3620\text{--}6900 \text{ \AA}$. The instrument rotator was set prior to each exposure, to align the slit within $\sim 2^\circ$ of the parallactic angle at the midpoint of the exposure. HeAr comparison spectra were taken immediately following each stellar exposure. The spectra were bias-subtracted, flat-fielded, background-subtracted, optimally extracted, wavelength-calibrated and flux-calibrated using standard IRAF tasks. Details of the individual low-resolution spectra are given in Table 4. The orbital phases in the last column are discussed in Section 5.1.

We acquired additional medium-resolution spectra in 2008 and 2009 for radial velocities, again with the B&C spectrograph on the 2.3 m Bok telescope. For these, we used an 832 mm^{-1} grating in second order with a $1''.5$ slit to achieve 1.8 \AA resolution over a wavelength range of $3675\text{--}4520 \text{ \AA}$. The slit was aligned with the parallactic angle at the midpoint of each exposure, the same as for the low-resolution spectra, but comparison HeAr spectra were taken before and after each stellar spectrum. The spectra were reduced in a similar manner, except that they were not flux-calibrated. After wavelength calibration, the radial velocity spectra were interpolated onto a log-wavelength scale. The continuum was removed from each spectrum by dividing through by a spline fit to the continuum, and then subtracting a constant equal to unity in order to get a continuum value of zero. Table 5 lists the details of the medium-resolution spectra. The radial velocities are described in Section 4.1 and the orbital phases in Section 5.1.

3.2. Differential Photometry

Differential *BVRI* light curves for 2M 1533+3759 were obtained at the Steward Observatory 1.55 m Kuiper telescope on Mt. Bigelow, Arizona between February and June of 2008 and in 2009 March. We used the Mont4K facility CCD camera⁸ with Harris *BVR* and Arizona *I* filters. Several hundred bias images and dome flats were obtained each day to reduce the error budget due to calibrations to less than 0.001 mag. The time stamp for each image is written by the clock on the CCD computer, which is synchronized with the on-site GPS system every 120 s, so that the times are always correct to better than a couple of tenths of a second. To reduce the observational sampling time, we used on-chip 3×3 binning and read out only 2/3 of the CCD rows, resulting in a readout time of 22 s per image. (For

Table 5
Medium Resolution 2.3 m Spectra and the Derived Radial Velocities

UT Date	HJD at midpoint (2450000+)	Exp Time (s)	S/N	V (km s^{-1})	V_{err} (km s^{-1})	Orbital Phase
2008 Feb 19	4516.02529	750	83.5	27.15	4.99	0.58
2008 Mar 18	4543.99112	550	80.7	-24.90	5.54	0.46
2008 Mar 18	4544.01329	550	80.0	30.54	4.73	0.59
2008 Mar 27	4552.97753	500	47.3	-9.29	6.68	0.01
2008 Apr 17	4573.93042	600	68.9	15.07	4.80	0.53
2008 Apr 18	4574.94859	550	61.3	68.75	5.65	0.82
2008 Apr 25	4581.88679	500	77.5	73.37	5.03	0.71
2008 Apr 25	4581.98355	625	79.0	-69.29	3.69	0.31
2008 Apr 26	4582.87608	550	77.9	55.20	3.76	0.83
2008 Apr 26	4582.96181	500	81.9	-57.65	3.96	0.36
2009 Feb 05	4868.02541	525	69.7	-2.92	4.54	0.51
2009 Mar 14	4904.83567	725	89.0	-34.43	4.18	0.05
2009 Mar 14	4904.84734	575	78.8	-50.58	3.84	0.13
2009 Mar 14	4904.85772	550	75.2	-68.20	4.23	0.19
2009 Mar 14	4904.86738	550	77.9	-78.37	4.74	0.25
2009 Mar 14	4904.87654	550	80.0	-71.28	4.86	0.31
2009 Mar 15	4905.83299	600	71.6	-66.07	4.46	0.22
2009 Mar 15	4905.84391	600	78.2	-76.04	5.03	0.29
2009 Mar 15	4905.89487	550	79.0	36.78	5.24	0.60
2009 Mar 15	4905.90420	500	75.8	60.08	4.26	0.66
2009 Mar 15	4905.91322	500	74.7	64.20	4.29	0.71
2009 Mar 15	4905.92344	500	74.0	66.27	4.19	0.78
2009 Mar 15	4905.93239	500	73.5	63.25	4.07	0.83
2009 Mar 15	4905.94190	500	71.5	43.94	3.87	0.89
2009 Mar 15	4905.95137	575	73.7	16.80	3.93	0.95
2009 Mar 15	4905.96212	700	59.1	-19.75	4.70	0.02
2009 Mar 15	4905.97491	625	78.1	-38.16	4.60	0.10
2009 Mar 16	4906.82916	575	89.5	-52.76	3.39	0.38
2009 Mar 16	4906.86126	525	86.6	27.75	4.86	0.57
2009 Mar 16	4906.87078	490	79.2	44.75	3.83	0.63
2009 Mar 16	4906.88020	490	80.5	62.30	4.13	0.69
2009 Mar 16	4906.88876	490	81.6	63.09	4.88	0.74
2009 Mar 16	4906.90777	490	82.3	51.32	3.20	0.86
2009 Mar 16	4906.91653	490	83.3	35.74	4.19	0.92
2009 Mar 16	4906.92530	490	70.8	19.09	4.43	0.97
2009 Mar 16	4906.93541	650	82.2	-22.00	4.08	0.03
2009 Mar 16	4906.94885	650	92.3	-48.09	3.14	0.12
2009 Mar 16	4906.97131	575	87.4	-74.59	4.20	0.25

2009, the readout time was reduced to 14 s, as a result of improvements to the electronics.) The remaining overhead time between images was 7 s, including 6 s for the filter change. We alternated between two filters each night in order to obtain two coeval light curves while maintaining adequate sampling of the eclipses. Table 6 summarizes the photometric observations.

The images were reduced with a pipeline constructed from standard IRAF tasks. The bias-subtracted images were flat-fielded with the appropriate *BVRI* dome flat and corrected for bad columns and cosmic rays. Images in the *I* filter were further corrected by subtracting a scaled, high S/N, zero-mean fringe frame. The fringe frame was constructed from 31 dithered *I* images, 600 s each, in fields with low stellar density, taken between 2008 March and May; the fringe pattern was very stable over that time interval. Aperture photometry was performed for the sdB and a set of reference stars, with the aperture radius set to 2.25 times the average FWHM in each image. The same set of eight, apparently nonvariable, reference stars was used with every filter; the reference stars were chosen to be distributed as closely and symmetrically as possible around 2M 1533+3759 (Figure 2). The differential magnitudes (sdB minus the average of the reference stars) were converted to relative fluxes and normalized to 1.0 near the quarter phase of the star's orbit.

⁸ See <http://james.as.arizona.edu/~psmith/61inch/instruments.html> for a description of the Mont4K CCD imager and filters.

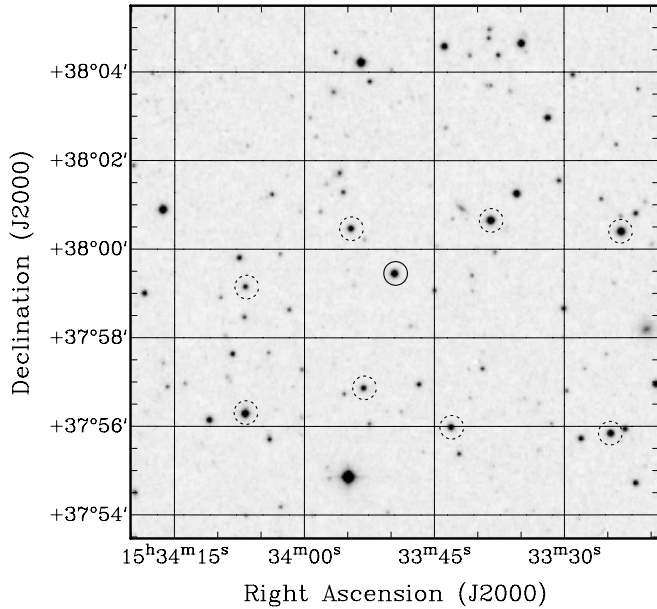


Figure 2. Finder chart for 2M 1533+3759. The solid circle in the center of the chart is 2M 1533+3759. The dashed circles are the adopted reference stars.

Table 6
Photometric Observations at the Steward Observatory
1.55 m Mt. Bigelow Telescope

UT Date	Start HJD (2450000+)	End HJD (2450000+)	Filter	Exp time (s)
2008 Feb 27	4523.879786	4523.982705	<i>B, R</i>	30, 25
2008 Feb 28	4524.943268	4525.031564	<i>B, R</i>	30, 25
2008 Mar 06	4531.902243	4532.025496	<i>B, R</i>	30, 25
2008 Mar 07	4532.896078	4533.016714	<i>B, R</i>	30, 25
2008 Mar 10	4535.898112	4536.025827	<i>B, R</i>	30, 25
2008 Mar 11	4536.942407	4537.022719	<i>B, R</i>	30, 25
2008 Mar 29	4554.843844	4555.016093	<i>B, R</i>	30, 25
2008 Apr 12	4568.787329	4568.974478	<i>V, I</i>	30,45
2008 Apr 13	4569.831345	4569.994764	<i>V, I</i>	30,45
2008 Apr 26	4582.818149	4582.981342	<i>V, I</i>	30,45
2008 Apr 27	4583.752365	4583.926433	<i>B, R</i>	35,30
2008 Jun 22	4639.674751	4639.710198	<i>B, R</i>	35,30
2009 Mar 28	4639.674751	4639.710198	<i>B, R</i>	30, 25

The resulting light curves, shown below in Figure 6 and further discussed in Section 7, have well-defined primary and secondary eclipses. The peak-to-peak amplitudes of the reflection effect are 0.10, 0.13, 0.15, and 0.19 mag, respectively, in the *BVRI* filters.

4. SPECTROSCOPIC ANALYSIS

4.1. Radial Velocities

We derived the radial velocities iteratively using a double-precision version of the IRAF task FXCOR. The initial velocity template was constructed by combining and median-filtering all 38 medium-resolution spectra. The individual spectra were cross-correlated against the template by fitting a Gaussian to the cross-correlation peak to determine the velocity shifts. The spectra were then Doppler-shifted to the same velocity and recombined into an improved template. Five iterations were required to reach convergence. Columns 5 and 6 in Table 5 list the derived radial velocities and their associated errors. Since FXCOR velocity errors are only known to within a

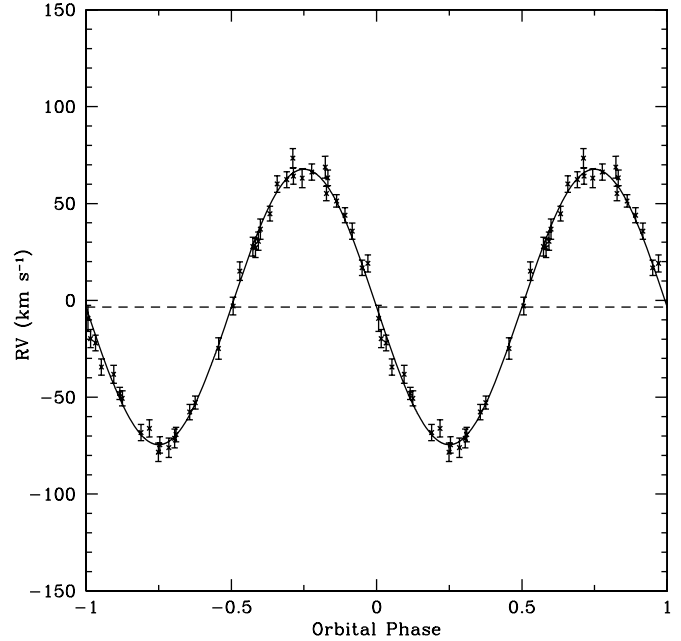


Figure 3. Radial velocity solution for 2M 1533+3759 as a function of orbital phase, superimposed on the observed velocities. The velocity amplitude and systemic velocity are $K_1 = 71.1 \pm 1.0 \text{ km s}^{-1}$ and $\gamma = -3.4 \pm 5.2 \text{ km s}^{-1}$.

scale factor, the final step was to scale the FXCOR errors so that the average error matches the standard deviation of the observed points about the fitted velocity curve.

The radial velocity solution was determined using a weighted least-squares procedure to fit a sine curve. The orbital period was fixed at the value derived from the eclipse times in the following section, since the photometric period is much more precise than the period derived from the velocities. The radial velocity solution is shown in Figure 3. The velocity semi-amplitude is $K_1 = 71.1 \pm 1.0 \text{ km s}^{-1}$. The systemic velocity, $\gamma = -3.4 \pm 5.2 \text{ km s}^{-1}$, was determined relative to three sdB radial velocity “standards,” PG 0101+039, PG 0941+280, and PG 2345+318, one or two of which were observed each night.⁹

4.2. Spectroscopic Parameters

We fit the Balmer lines from $H\beta$ to H_{11} and the strongest helium lines (4922 Å, 4471 Å, and 4026 Å) in our low-resolution spectra to synthetic line profiles calculated from a grid of zero-metallicity non-LTE (NLTE) atmospheric models. Our expectation was that the reflection effect in 2M 1533+3927 would introduce negligible contamination from the secondary. The only sdB+dM binary whose spectroscopic parameters have previously been reported to vary with orbital phase is HS 2333+3927 (Heber et al. 2004), and its reflection effect is more than twice as large as that of 2M 1533+3927. We were therefore surprised to find that our individual low-resolution spectra for 2M 1533+3927 do in fact give significantly different temperatures at different orbital phases, amounting to the better part of 1000 K.

We therefore returned to our more numerous medium-resolution spectra, and (after reinterpolating onto a linear wavelength scale) fit $H\gamma$ through H_{11} , He 4471 Å, and 4026 Å, again using zero-metallicity NLTE models. The medium-resolution

⁹ These are actually short-period sdB+WD binaries with large velocity amplitudes that we have observed for 10–15 years, whose velocities are known to 1–2 km s^{-1} at any given time.

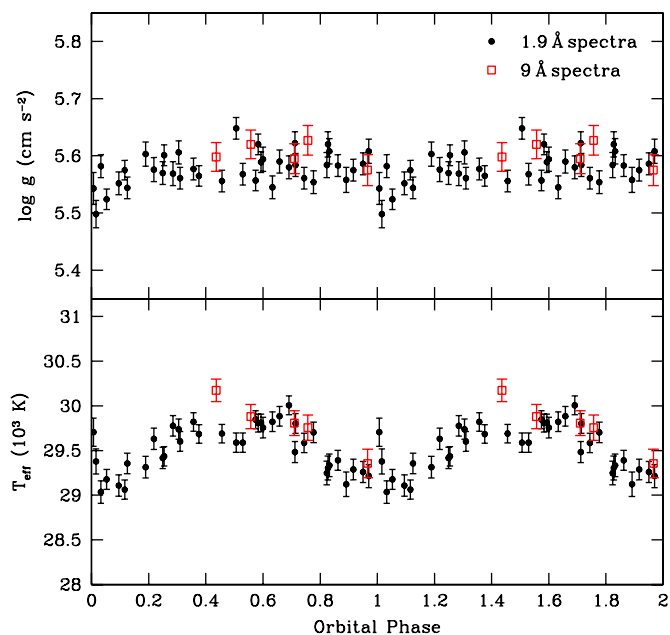


Figure 4. Derived gravities (above) and effective temperatures (below) as a function of orbital phase, from fits to Balmer and helium lines in 2M 1533+3759.

spectra show the same orbital temperature effect (Figure 4), with about the same amplitude, even though they exclude H β (which suffers the most from contamination by the secondary of all the lines we considered). The lowest derived temperatures are found from spectra taken near minimum light. The unexpected prominence of the temperature variations with orbital phase is probably due to the high S/N noise of our spectra (70–90 per pixel). There is also a suggestion of a similar trend with gravity, but the derived helium abundances were negligibly affected. (For unknown reasons, our temperature variations are in the same sense as those derived by Heber et al. (2004) using only helium lines (their Figure 7(b)), and in the opposite sense from what they found when fitting both Balmer and helium lines, although naturally we see smaller amplitude variations for 2M 1533+3759.)

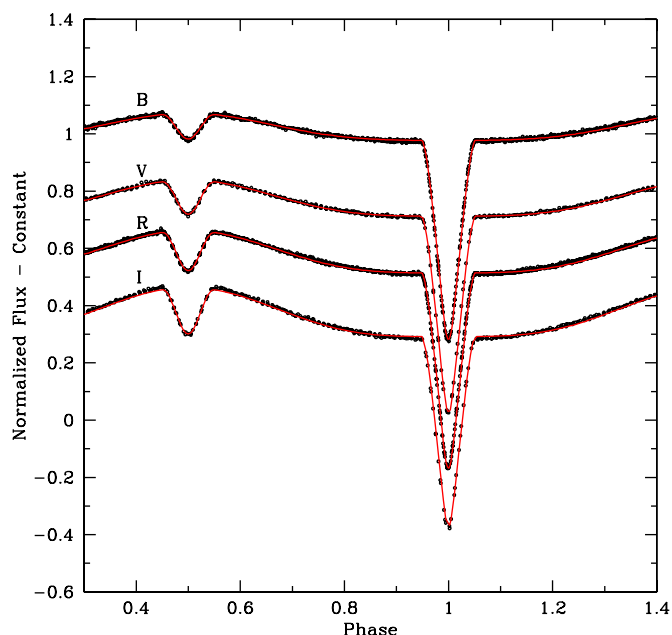


Figure 6. Observed light curves superimposed onto the calculated theoretical light curves (solid red lines). The *VRI* light curves are each offset by a constant with respect to the *B* light curve.

To be safe, we adopted atmospheric parameters determined from 14 spectra observed near minimum light, i.e., orbital phases between 0.8 and 1.2, not including the two points closest to the center of the primary eclipse. (The temperature derived at the mid-point of the primary eclipse was surprisingly discrepant, possibly due to absorption of some of the unclipped sdB light near the limb of the secondary; discrepant gravity values were also seen during both eclipses.) The excellent quality of the fit can be seen in Figure 5. Our adopted spectroscopic parameters are $T_{\text{eff}} = 29230 \pm 125$ K, $\log g = 5.58 \pm 0.03$, and $\log N(\text{He})/N(\text{H}) = -2.37 \pm 0.05$, where the errors are the standard deviations of the values from the individual spectra. This T_{eff} was used as the initial value for the primary temperature in our light-curve modeling in Section 5.2.

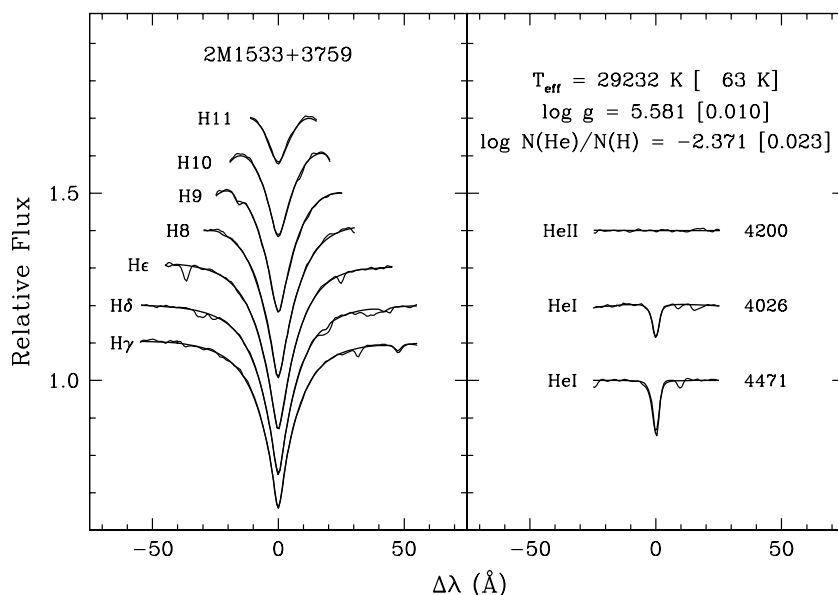


Figure 5. Fits of the Balmer and helium lines in the combined 2M 1533+3759 minimum light spectrum to synthetic zero-metallicity NLTE line profiles.

Table 7
Times of Minima of 2M 1533+3759

Mid Eclipse (HJD 2450000+)	Error	Epoch	Type	Filter	$O - C$ (s)
4523.93875	2.5×10^{-5}	-0.5	Sec.	<i>R</i>	7.2
4524.99017	1.5×10^{-5}	6.0	Pri.	<i>R</i>	-0.4
4531.94631	1.5×10^{-5}	49.0	Pri.	<i>R</i>	0.6
4532.91693	1.5×10^{-5}	55.0	Pri.	<i>R</i>	0.4
4532.99788	2.5×10^{-5}	55.5	Sec.	<i>R</i>	6.0
4535.90970	2.5×10^{-5}	73.5	Sec.	<i>R</i>	1.9
4535.99054	1.5×10^{-5}	74.0	Pri.	<i>R</i>	-2.0
4536.96115	1.5×10^{-5}	80.0	Pri.	<i>R</i>	-3.1
4554.91769	1.5×10^{-5}	191.0	Pri.	<i>R</i>	-1.1
4554.99860	2.5×10^{-5}	191.5	Sec.	<i>R</i>	1.0
4568.82995	1.5×10^{-5}	277.0	Pri.	<i>V</i>	-0.8
4568.91082	2.5×10^{-5}	277.5	Sec.	<i>V</i>	-2.1
4569.88151	2.5×10^{-5}	283.5	Sec.	<i>V</i>	3.7
4569.96228	1.5×10^{-5}	284.0	Pri.	<i>V</i>	-6.2
4582.82312	2.5×10^{-5}	363.5	Sec.	<i>V</i>	1.7
4582.90399	1.5×10^{-5}	364.0	Pri.	<i>V</i>	0.3
4583.79377	2.5×10^{-5}	369.5	Sec.	<i>R</i>	4.0
4583.87460	1.5×10^{-5}	370.0	Pri.	<i>R</i>	-0.7
4639.68546	1.5×10^{-5}	715.0	Pri.	<i>R</i>	4.8
4918.90113	1.5×10^{-5}	2441.0	Pri.	<i>R</i>	-2.1
4918.98208	2.5×10^{-5}	2441.5	Sec.	<i>R</i>	3.5

5. PHOTOMETRIC ANALYSIS

5.1. Ephemeris

We solved for the orbital period using a linear least-squares fit to the well-defined times of primary and secondary eclipse minima in the *V* and *R* light curves, in the equation $T_{\min} = T_0 + nP$, where T_{\min} are the times of the eclipse minima, T_0 is the reference HJD for the primary eclipse at $n = 0$, n are the cycle numbers, and P is the orbital period in units of a day.

The time of minimum for each observed primary and secondary eclipse was determined by fitting an inverse Gaussian to the eclipse shape. The results are listed in Table 7, along with the corresponding cycle numbers, the instrumental filter, and the $O - C$ time residuals. The standard deviation of the $O - C$ values is 3.3 s. The derived ephemeris for the primary eclipses is

$$\text{HJD} = (2454524.019552 \pm 0.000009) \\ + (0.16177042 \pm 0.00000001) \times E.$$

5.2. Light-curve Modeling

The *BVRI* light curves were phased with the ephemeris and orbital period derived from the photometry. Small vertical flux differences equivalent to a few hundredths of a magnitude remained in the phased light curves. These could be due to slight long-term variability in one or more of the reference stars, but are more likely to be caused by subtle variations in the dome flats from different runs. We therefore shifted the light curves in the same filter vertically by a small constant to minimize the standard deviation of the total phased light curves for that filter. The light curves for all four filters were analyzed simultaneously with the MOdified ROche (MORO) code (Drechsel et al. 1995).

The MORO code adopts the Wilson–Devinney monochromatic light, synthetic light-curve calculation approach (Wilson & Devinney 1971), but has implemented a modified Roche model that takes into account radiation pressure effects in close binaries with hot components. It also replaces the classical

Wilson–Devinney grid search differential corrections method with a more powerful *SIMPLEX* optimization algorithm. This provides several advantages: in particular, the fitting procedure improves with each iteration and is not allowed to diverge. For details of the numerical procedure and the radiation pressure implementation, we refer the reader to the description in Drechsel et al. (1995).

Light-curve modeling becomes a challenging task when information about the secondary is limited, as is the case in all single-lined spectroscopic binaries. Since the modeling requires a large set of parameters, it is important to constrain as many as possible based on additional spectroscopic and theoretical information. We assumed the orbit is circular, and the stellar rotation is synchronized with the orbit, since the timescales for both circularization and synchronization are a few decades (Zahn 1977), very much shorter than the helium burning lifetime of a horizontal branch star. We adopted the spectroscopic T_{eff} of the sdB as an initial parameter, and took the linear limb-darkening coefficients (x_1) of 0.305, 0.274, 0.229, and 0.195 from Diaz-Cordoves et al. (1995) and Wade & Rucinski (1985) for the *B*, *V*, *R*, and *I* filters, respectively. These values correspond to the nearest available stellar atmosphere model, a star with $T_{\text{eff}} = 30,000$ K and $\log g = 5.0$, and should be very close to the correct values (Wood et al. 1993), since the dependence on the surface gravity is weak. Previous experience with light-curve modeling of similar systems (Hilditch et al. 1996) indicates that the limb-darkening coefficient of the cool secondary star (x_2) can deviate highly from normal values for cool dwarf stars, so we decided to treat x_2 as an adjustable parameter. Due to the irradiation effect, the limb darkening can be expected to be more extreme than for single stars, and thus we employed initial values of 0.7, 0.8, 1.0, and 1.0, for the *B*, *V*, *R*, and *I* filters, respectively. The primary albedo (A_1) was fixed to 1.0, and its gravity darkening exponent (β_1) was set to 1.0, appropriate for a radiative outer envelope (von Zeipel 1924). The enormous reflection effect suggests a mirror-like surface on the heated side facing the primary, indicating complete reradiation of the primary light; therefore, a secondary albedo (A_2) of 1.0 was adopted. We set the gravity-darkening exponent (β_2) to 0.32 for the convective secondary (Lucy 1967). The radiation pressure parameter for the secondary star (δ_2) was set to zero because the radiation pressure forces exerted by the cool companion are negligible. A blackbody approximation was used to treat the irradiation of the secondary by the primary. We input central wavelengths of 4400, 5500, 6400, and 7900 Å for our *BVRI* passbands, which are a fair match to the filter passbands convolved with the CCD sensitivity.

The simultaneous light-curve modeling was performed with the Wilson–Devinney mode 2 option, for a detached system. The remaining free parameters for the fitting procedure include the orbital inclination, i ; the effective temperature of the secondary, T_2 ; the Roche surface potential, Ω_1 and Ω_2 ; the mass ratio, $q = M_2/M_1$; the color-dependent luminosity of the primary, L_1 ; the radiation pressure parameter for the primary, δ_1 ; and l_3 , a potential third light contribution due to a possible unresolved field star or an extended source. The color-dependent luminosity of the secondary, L_2 , was not adjusted but was recomputed from the secondary’s radius and temperature.

Degeneracy is a common problem encountered in light-curve modeling. A high degree of correlation between several parameters (e.g., i , q) can result in several equally good solutions with different families of parameters. Therefore, it is necessary to test for the presence of multiple good solutions over a

wide range of mass ratios. The usual procedure is to run a series of initial trials at discrete mass ratios, keeping them fixed. Unfortunately, our first set of trials did not produce any good solutions for mass ratios in the range $1.2 < q < 0.2$, corresponding to either an sdB mass of $0.49 M_{\odot}$ and M dwarf masses in the range $0.6\text{--}0.1 M_{\odot}$ (M0–M5.5), or to smaller sdB masses and later M spectral types—i.e., there were no solutions that matched the shapes of our observed light curves—because the reflection effect was underestimated by about 30% in all of the models. The trial runs did however suggest that there was no third light contribution, so we set that parameter to zero for the rest of the runs.

A similar, although less extreme, problem was encountered in previous attempts to model the light curves of eclipsing sdB+dM binaries (Kilkenny et al. 1998, PG 1336–018; Drechsel et al. 2001, HS 0705+6700), especially with redder filters, and for the same reason: theoretical models are not sophisticated enough in their treatment of the reflected/reradiated light. Both Kilkenny et al. (1998) and Drechsel et al. (2001) found that if the secondary albedo was treated as a free parameter, their solutions converged to physically unrealistic values, $A_2 > 1.0$, although they were able to find acceptable solutions when A_2 was held fixed at a value of 1.0. Vučković et al. (2007) and Lee et al. (2009), both using Wilson–Devinney synthesis codes, noted that their biggest difficulty concerned the temperature of the heated secondary. This appears to be an alternate version of the same basic problem, i.e., correctly treating the light from the secondary star, which manifests differently in different adaptations of the Wilson–Devinney code. Vučković et al. (2007) were able to find good solutions with $A_2 = 0.92$ by simply fixing their secondary temperature at the average of the values found separately in their two passbands. Lee et al. (2009) had to resort to mode 0 instead of mode 2, allowing L_2 and T_2 to be separate free parameters (rather than computing L_2 from T_2 and R_2), in addition to fixing $A_2 = 1.0$. Since we could not find any acceptable fits to our light curves with MORO when A_2 was set to 1.0, we decided to treat it as an adjustable scale factor, accepting that it would converge to an unphysically high value.

When A_2 was no longer kept fixed, good fits to the light-curve shapes were found for the following mass ratios: $q = 0.301, 0.586, 0.697, 0.800, \text{ and } 0.888$. To discriminate between the possible solutions, we calculated the sdB mass corresponding to each value of q , using the mass function, which can be expressed as

$$\frac{M_1 \times (q \sin i)^3}{(1+q)^2} = \frac{K_1^3 P}{9651904}, \quad (1)$$

where i is the corresponding inclination angle, which was always $86^{\circ}6 \pm 0^{\circ}2$, and with $K_1 = 71.1 \text{ km s}^{-1}$ and $P = 0.16177042$ day, as derived above. The resulting sdB masses are 0.376, 0.076, 0.052, 0.038, and $0.031 M_{\odot}$, respectively. According to evolutionary models, core helium burning sdB stars must have masses substantially larger than $0.08 M_{\odot}$, leaving only one reasonable solution, $q = 0.301$.

Once q was constrained to a single approximate value, the problem was reduced to finding the deepest minimum in the surrounding multidimensional parameter space. The *SIMPLEX* algorithm is a very powerful numerical tool, but it is always possible for any algorithm to converge into a less-than-optimal local minimum. To verify that the converged $q = 0.301$ solution was the deepest minimum in the local vicinity, we varied the set of starting parameters over $0.27 < q < 0.35$ ($0.26 M_{\odot} < M_1 < 0.50 M_{\odot}$) in multiple additional runs, to make sure that they all

Table 8
Light Curve Solution for 2M 1533+3759 and Goodness of Fit

Parameter	Values
Fixed Parameters	
β_1^a	1.0
β_2^a	0.32
A_1^b	1.0
$x_1(B)^c$	0.305
$x_1(V)^c$	0.274
$x_1(R)^c$	0.229
$x_1(I)^c$	0.195
δ_2^d	0.0
$l_3(B, V, R, I)^e$	0.0
Adjusted Parameters	
i	$86^{\circ}6 \pm 0^{\circ}2$
A_2^b	2.0 ± 0.2
$q(M_2/M_1)$	0.301 ± 0.014
Ω_1^f	6.049 ± 0.230
Ω_2^f	3.305 ± 0.098
δ_1^d	0.035 ± 0.043
$T_{\text{eff}}(1)$	30400 ± 500
$T_{\text{eff}}(2)$	3100 ± 600
$x_2(B)^c$	0.83 ± 0.17
$x_2(V)^c$	0.91 ± 0.09
$x_2(R)^c$	0.95 ± 0.05
$x_2(I)^c$	1.00 ± 0.02
$L1(B)^g$	0.99996 ± 0.00004
$L1(V)^g$	0.99978 ± 0.00017
$L1(R)^g$	0.99941 ± 0.00043
$L1(I)^g$	0.99821 ± 0.00116
Fractional Roche Radii^h	
$r_1(\text{pole})$	0.168 ± 0.003
$r_1(\text{point})$	0.169 ± 0.003
$r_1(\text{side})$	0.168 ± 0.002
$r_1(\text{back})$	0.169 ± 0.002
$r_2(\text{pole})$	0.153 ± 0.001
$r_2(\text{point})$	0.154 ± 0.004
$r_2(\text{side})$	0.154 ± 0.001
$r_2(\text{back})$	0.157 ± 0.003
Standard Deviation	
σ_B	0.0072
σ_V	0.0061
σ_R	0.0069
σ_I	0.0080

Notes.

- ^a Gravity darkening exponent
- ^b Bolometric albedo
- ^c Limb darkening coefficient
- ^d Radiation pressure parameter
- ^e Fraction of third light at maximum
- ^f Roche surface potential
- ^g Relative luminosity, $L_1/(L_1 + L_2)$
- ^h In units of separation of mass centers

converged to the same solution within a small error margin, which they did. Table 8 lists the best light-curve solution for 2M 1533+3759 for all the filters. The standard deviations of the various fits are at the bottom. The observed *BVRI* light curves are shown together with the calculated theoretical curves in Figure 6.

Throughout the previous runs, the temperature of the primary, T_1 , was initialized to the spectroscopic value, but it was allowed to be an adjustable parameter. The converged results showed a consistent preference for a higher-than-observed effective temperature by 1200 K or so. However, once we isolated the

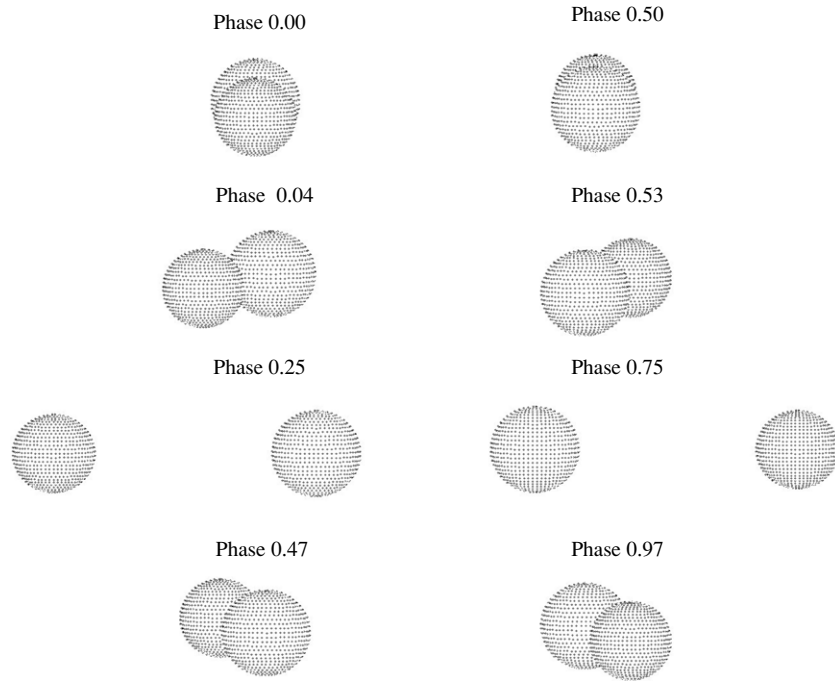


Figure 7. Snapshots of 2M 1533+3759 at various orbital phases, as viewed from an inclination angle of $86^\circ.6$. Left column, top to bottom: phase 0.00 (primary eclipse), 0.04, 0.25, and 0.47. Right column, top to bottom: phase 0.50 (secondary eclipse), 0.53, 0.75, and 0.97.

best model, we reran the solution while keeping T_1 fixed at 29,230 K. The resulting values of the mass ratio, inclination angle, fractional radii, etc., in Table 8 are the same, within the errors, whether T_1 is 30,400 K or 29,230 K.

Figure 7 is a series of snapshots from a three-dimensional animation of 2M 1533+3759 at different orbital different phases.

6. GEOMETRY AND SYSTEM PARAMETERS

The light-curve solution allows us to calculate the absolute system parameters. Substituting the values of K_1 and P from Sections 4.1 and 5.1 into Equation (1), along with $q = 0.301$ and $i = 86^\circ.6$, results in component masses $M_1 = 0.376 \pm 0.055 M_\odot$ and $M_2 = 0.113 \pm 0.017 M_\odot$. Kepler’s law tells us that the orbital separation, a , is $0.98 \pm 0.04 R_\odot$, which can then be used to scale the fractional radii from the model solution in order to get the actual radii, $R_1 = 0.166 \pm 0.007 R_\odot$ and $R_2 = 0.152 \pm 0.005 R_\odot$.

The light-curve modeling is completely independent of the observed spectroscopic gravity, which therefore provides a nice consistency check. The calculated $\log g$ corresponding to our derived M_1 and R_1 turns out to be 5.57 ± 0.07 , essentially identical with our adopted spectroscopic value of 5.58.

In the past, error bars have not usually been attached to masses derived from modeling light curves of sdB+dM binaries, but we found it to be a very instructive exercise. The formal error propagation for the primary mass, according to Equation (1), includes the uncertainties on q , i , K_1 , and P . Although the mass depends on the cubic power of both K_1 and q , the error in K_1 is small enough in our case that the mass uncertainties are dominated by the uncertainty in q , as small as it is. Ninety five percent of the error in M_1 is due to the $3M_1\Delta q/q$ term. Our inability to more tightly constrain the sdB mass is a dramatic illustration of why useful mass constraints from light-curve modeling can usually be obtained only for eclipsing systems (unless, of course, good radial velocities can be obtained from both components). Furthermore, even with an eclipsing sdB+dM

binary, the light-curve shapes and velocity amplitude must be sufficiently precisely observed to adequately minimize the other error terms, or else the uncertainty in the mass will be even larger.

The temperature of the secondary is somewhat more uncertain, 3100 ± 600 K, since it contributes almost negligibly to the total light, aside from the reflection effect. Nevertheless, our model value for T_2 is quite acceptable. According to the theoretical T_{eff} —mass—luminosity relation of Baraffe & Chabrier (1996), the predicted temperature and radius of a $0.113 M_\odot$ main-sequence star should be 2854 K and $0.138 R_\odot$, respectively, corresponding to an M5 dwarf. The empirical mass—radius relation of Bayless & Orosz (2006) for low-mass main-sequence stars gives an identical radius of $0.138 R_\odot$. Our value of $0.152 R_\odot$ is slightly larger (although still within the 3σ error), but it would not be unexpected if the highly heated and already slightly distorted secondary in a system like 2M 1533+3759 turned out to be a little larger than an isolated M dwarf of the same mass.

Table 9 summarizes the system parameters for 2M 1533+3759, beginning with our adopted spectroscopic parameters and the photometric and radial velocity solutions described in the previous sections.

7. DISCUSSION

We examined several possible systematic effects, beginning with our spectroscopic parameters. Under the reasonable assumption that the primary’s rotation is synchronized with the orbital period, its rotational velocity should be $V_{\text{rot}_1} = 2\pi R_1/P = 52 \pm 2 \text{ km s}^{-1}$. This corresponds to 1.0 pixel in our medium-resolution spectra, which have an instrumental FWHM of 2.75 pixels. We reanalyzed our combined minimum-light spectrum after broadening the synthetic spectra by this extra amount, and found that the expected rotation has a negligible effect on the spectroscopic parameter determination. The derived temperature was reduced by 10 K and the gravity was reduced by 0.002 dex.

Table 9
Fundamental Parameters of 2M 1533+3975

Parameter	Values
$T_{\text{eff}1}$ (K)	29230 ± 125
$\log g$ (cm s $^{-2}$)	5.58 ± 0.03
$\log N(\text{He})/N(\text{H})$	-2.37 ± 0.05
Period (days)	$0.16177042 \pm 0.00000001$
T_0 (days)	$2454524.019552 \pm 0.000009$
K_1 (km s $^{-1}$)	71.1 ± 1.0
γ (km s $^{-1}$)	-3.4 ± 5.2
M_1 (M_{\odot})	0.376 ± 0.055
M_2 (M_{\odot})	0.113 ± 0.017
a (R_{\odot})	0.98 ± 0.04
R_1 (R_{\odot})	0.166 ± 0.007
R_2 (R_{\odot})	0.152 ± 0.005
$T_{\text{eff}2}$ (K)	3100 ± 600
$V_{\text{rot}1}$ (km s $^{-1}$)	52 ± 2
L_1 (L_{\odot})	18.14 ± 1.84
M_{V_1}	4.57 ± 0.21
d (pc)	644 ± 66

Next, we investigated the effects of using zero-metallicity NLTE atmospheres to derive our spectroscopic parameters, since metal lines are observed to be present in sdB atmospheres, especially in the UV. Two of us (G.F. and P.C.) conducted an experiment in which TLUSTY was used to construct a synthetic model atmosphere at a temperature of 28,000 K, $\log g = 5.35$, $\log N(\text{He})/N(\text{H}) = -2.70$, and solar abundances of C, N, O, S, and Fe. Using our zero-metallicity NLTE grid, the derived parameters were found to be $T_{\text{eff}} = 30,096$ K, $\log g = 5.54$, and $\log N(\text{He})/N(\text{H}) = -2.72$. At these abundances, we would have overestimated the effective temperature by about 2000 K and the surface gravity by almost 0.2 dex, so the true values for 2M 1533+3759 would be about 27,300 K and 5.40, respectively. Happily, the light-curve solution is amazingly robust. The model results obtained by further lowering the primary temperature to a fixed value of 27,300 K are only negligibly different from our original solution. Thus, the system parameters would remain essentially the same: $q = 0.303$, $i = 86^{\circ}.5$, $M_1 = 0.370 M_{\odot}$, $M_2 = 0.112 M_{\odot}$, $R_1 = 0.165 R_{\odot}$, $R_2 = 0.152 R_{\odot}$, and $a = 0.98 R_{\odot}$. The calculated sdB surface gravity would also be unchanged, $\log g = 5.57 \pm 0.03$, but would no longer be as consistent with the expected gravity of 5.40. This implies that the atmospheric abundances in 2M 1533+3759 are not as large as the solar values assumed above.

We spent considerable time worrying about the very large secondary albedo, $A_2 \sim 2$, that was required to obtain a solution which fits the observed shapes of the 2M 1533+3759 light curves, since all previous sdB+dM analyses were able to find acceptable light-curve solutions with $A_2 \sim 1$. We tested the version of MORO running at the University of Texas using Drechsel et al.'s (2001) input datafile, and found exactly the same solution that they did. We verified that an independent Steward V light-curve data for HS 0705+6700, in the same format as our 2M 1533+3759 data, produced a curve that fell exactly between Drechsel et al.'s (2001) normalized B and R data for HS 0705+6700, thus eliminating problems with our input format. We shifted the $BVRI$ effective wavelengths specified to MORO by up to 200 Å, with no effect on the output solution.

Our data set is unique among published sdB+dM light-curve analyses in extending to the I filter. Drechsel et al. (2001) fit only B and R data, Heber et al. (2004) fit BVR , Vučković et al.

(2007) used g' (intermediate between B and V) and r' (close to R), and Lee et al. (2009) had only V and R . We therefore reanalyzed our 2M 1533+3759 data using only the B and R light curves. The results were the same as before: when A_2 is allowed to be a free parameter, the solution always converges to A_2 near 2. Furthermore, no new solutions appear for other q values, and the solution for $q = 0.301$ is nearly identical to our previous best solution. If A_2 is forced to have a value of 1, the B and R solutions fail to fit the observed light-curve shapes in nearly the same manner as our original trial solutions at the same A_2 and q . The amplitude of the theoretical reflection effect with $A_2 = 1$ using current models simply is not large enough to fit 2M 1533+3759.

An alternate way to look at this problem is to compare the reflection effect amplitudes in 2M 1533+3759 versus HW Vir. HW Vir was selected because it has the next longest orbital period of well-studied eclipsing sdB+dM systems besides 2M 1533+3759, and because our high S/N spectra give essentially identical temperatures and gravities for these stars when analyzed in a homogeneous manner. However complicated the physics of the reflection effect may be, the actual processes ought to be similar in both systems. Thus, to first order, the reflection effect amplitudes should be proportional to the luminosity of the primary and the surface area of the heated face of the secondary, and inversely proportional to the distance between the two stars. Using our values of R_1 , $T_{\text{eff}1}$, R_2 , and a for 2M 1533+3759, and Lee et al.'s (2009) values for HW Vir ($0.183 R_{\odot}$, 28,490 K, $0.175 R_{\odot}$, and $0.86 R_{\odot}$, respectively) to calculate the ratio of $R_1^2 T_{\text{eff}1}^4 R_2^2 / a^2$ for the two binaries, we find that the amplitude in 2M 1533+3759 ought to be 53% of the amplitude in HW Vir. Instead, it is observed to be 95% of the HW Vir amplitude. It seems that the reflection effect in 2M 1533+3759 really is stronger than would be expected, compared to other known eclipsing sdB+dM binaries. Another light-curve solution might give a different result, but an exhaustive search of parameter space failed to find any other solution that fit our data.

The most interesting result of our modeling is the unusually low mass obtained for the sdB star in 2M 1533+3759. The vast majority of sdB masses derived previously from asteroseismology of sdB pulsators (Table 1) or by modeling sdB+dM binaries (Table 2) are clustered near the canonical value of $0.48 M_{\odot}$, i.e., near the mass of the degenerate He core at helium ignition in low-mass red giants. However, there are at least one or two other hot subdwarfs for which masses lower than $0.4 M_{\odot}$ have also been found.

The first anomalously low mass for a hot subdwarf was found for the eclipsing sdO+dM binary, AA Dor, although this result continues to be the subject of debate (Rucinski 2009; Fleig et al. 2008; Vučković et al. 2008, and references therein). The most recent values for the sdO mass, $0.25 M_{\odot}$ (Rucinski 2009) and $0.24 M_{\odot}$ (from Fleig et al.'s values for the surface gravity, 5.30, and radius, $0.181 R_{\odot}$) are too low for a core helium burning star, implying that AA Dor is on a post-RGB cooling track, as originally suggested by Paczynski (1980). This is consistent with the fact that AA Dor (42,000 K) is much hotter than sdB stars.

Heber et al. (2004, 2005) used the MORO code to model light curves of HS 2333+3927, the non-eclipsing sdOB+dM binary with the largest known reflection effect, and found two good solutions with quite different secondary albedos, $A_2 = 0.39$ and $A_2 = 1.00$. Interestingly, their spectroscopic $\log g$ and mass-radius relations convincingly argued that the lower albedo

solution should be preferred—the opposite of what has been required for all other sdB+dM light-curve modeling—resulting in a primary mass of $0.38 \pm 0.09 M_{\odot}$ for HS 2333+3927. However, Heber et al. pointed out that a mass of $0.47 M_{\odot}$ corresponds to $\log g = 5.86$, only 0.16 dex larger than their observed spectroscopic $\log g = 5.70$, leaving room for doubt about the mass. While it is clear that a non-eclipsing system is inherently more uncertain than an eclipsing one, there are two further pieces of evidence in favor of a lower mass for HS 2333+3927. Heber et al.’s gravity was derived using zero-metallicity NLTE atmospheres, and if the metallicity corrections at 36,000 K go in the same direction as they do at several thousand degrees cooler, then any such corrections should reduce the gravity, and therefore lower the derived mass. We can also corroborate their observed surface gravity from our own independent measurements of multiple high S/N spectra taken within 15 minutes of the minimum of the reflection effect (Green et al. 2008), similarly analyzed with zero-metal NLTE synthetic atmospheres. While optical spectra are not as free from the secondary contamination as ultraviolet spectra, our derived $\log g$ of 5.70 is nevertheless identical to Heber et al.’s value, supporting their lower value for the mass. (Heber et al. alternately suggested that HS 2333+3927 might be on a post-RGB cooling track, although that would require an even lower mass of $0.29 M_{\odot}$.)

Østensen et al. (2008) reported a very low mass ($<0.3 M_{\odot}$) for the eclipsing sdB, HS 2231+2441, but their result is rather uncertain, as it depends strongly on the spectroscopic $\log g = 5.39$, which was determined using solar abundances. Our independent estimate of the gravity for this star, using the same homogeneous zero-metal NLTE atmospheric models that we used for 2M 1533+3927 and HS 2333+3927, is 5.51, consistent with a mass of $0.47 M_{\odot}$. The true value is presumably somewhere in between. Further investigation is required to better assess the sdB mass in HS 2231+2441.

Randall et al. (2007) utilized the completely different technique of asteroseismology to derive a mass of $0.39 \pm 0.01 M_{\odot}$ for the *p*-mode sdB pulsator, PG 0911+456. The high precision is due to the fact that the envelope pulsations are extremely sensitive to the surface gravity. It turns out that any systematic metallicity corrections would also tend to reduce the mass in this case, as well. This is because the asteroseismic models were calculated for a fixed temperature, the observed spectroscopic value of 31940 K, which was once again determined by fits to synthetic zero metal NLTE atmospheres. There is a known degeneracy in mass versus temperature (and gravity) for similar sdB asteroseismic solutions (Charpinet et al. 2005b). For PG 0911+456, every 400 K decrease in the assumed effective temperature due to metallicity corrections would lower the derived sdB mass by about $0.01 M_{\odot}$.

Given the robustness of our light-curve solution, the mass of $0.376 \pm 0.055 M_{\odot}$ for 2M 1533+3927 appears rather firm. Thus, there is now significant evidence from two completely independent observational and analytical techniques, asteroseismology and light-curve modeling in binary stars, for the existence of sdB stars with masses around $0.38 M_{\odot}$.

Even one or two sdB stars with masses less than 0.40 – $0.43 M_{\odot}$, out of about 16 whose masses are fairly well determined, constitute an important fraction. One such star might conceivably lie on a post-RGB cooling track but the odds are very much against it. For example, 2M 1533+3927, PG 0911+456, and HS 2333+3927 all fall near the extremely fast loop at the beginning of Althaus et al.’s (2001) $0.406 M_{\odot}$

cooling track (between C and D in their Figure 1), but the few years spent in that early phase are insignificant compared to typical core helium burning lifetimes ($\sim 10^8$ yr). The only post-RGB stars with any reasonable likelihood of being seen at the temperatures and gravities of typical sdB stars have masses less than $0.30 M_{\odot}$ (Althaus et al. 2001; see also Figure 10 of Heber et al. 2004). The evidence therefore suggests that sdB stars with masses near $0.38 M_{\odot}$ are bona fide core helium burning horizontal branch stars.

The mass of PG 0911+456 is more precisely known and therefore the evolutionary history is more interesting. It does not now appear to be in a binary system (Randall et al. 2007), and it is not clear why some, but not all, single $\sim 2 M_{\odot}$ progenitors would lose their entire envelopes. The merger of two helium white dwarfs is not a completely satisfactory alternative—Han et al.’s sdB models give a lower limit of $0.4 M_{\odot}$ for the product of such a merger—unless some of the mass in the two white dwarfs can somehow manage to escape during the merger. Politano et al.’s (2008) common envelope merger model predicts a lower mass limit ($\leq 0.32 M_{\odot}$) in better agreement with the observed mass of PG 0911+456. Their model also hypothesizes that since fast rotators lose more envelope mass, a significant fraction of the envelope angular momentum would be carried away, slowing down the star’s rotation. However, PG 0911+456 has an unusually low rotational velocity, less than 0.1 km s^{-1} , and it is not clear if a common envelope merger could explain the loss of essentially all the envelope mass as well as nearly all the angular momentum.

2M 1533+3759 has clearly been through an initial common envelope. Theoretical investigations, from the first in-depth study by Sweigart et al. (1989) to recent work aimed specifically at binary systems expected to produce hot subdwarfs (Han et al. 2002, 2003; Hu et al. 2007), indicate that helium burning cores somewhat less than $0.40 M_{\odot}$ are produced by stars with initial masses greater than about $2 M_{\odot}$, which undergo non-degenerate helium ignition. Of course, 2M 1533+3759 might still have had a degenerate helium flash if the mass of the sdB is toward the upper end of the possible range. Still, either way, a helium core mass less than about $0.43 M_{\odot}$ ought to have evolved from a main-sequence progenitor with an initial mass of at least 1.8 – $2.0 M_{\odot}$, which corresponds to a main-sequence A star (Binney & Merrifield 1998). 2M 1533+3759 therefore presents the best observational evidence so far that stars with initial main-sequence masses this large can be sdB progenitors. (The situation in sdB binaries with compact companions is less clear, since mass may have been transferred to the sdB progenitor during the evolution of the original primary.)

Previously, the upper limit to the mass of an sdB progenitor could only be estimated from the fact that sdB stars have not been found in any galactic clusters younger than NGC 188, which has an age of 6–7 Gyr and a turnoff mass of $1.1 M_{\odot}$ (Meibom et al. 2009). Small number statistics clearly play an important role here, since there are only two hot subdwarfs in NGC 188, and half a dozen or so in NGC 6791 (Landsman et al. 1998), the only other old open cluster known to contain such stars, and the majority of younger open clusters are even less massive than these two.

Indeed, at a mass of $0.38 M_{\odot}$, 2M 1533+3759 (and perhaps also HS 2333+3927, if the latter’s mass is in fact less than $0.4 M_{\odot}$) would fall at the low-mass end of Han et al.’s (2003) preferred distribution for the first common envelope ejection channel (see their Figure 12). The existence of a binary like 2M 1533+3759 therefore may also provide support for Han

et al's (2002, 2003) assumption that a fraction of the ionization energy contained in the progenitor red giant's envelope combines with the liberated gravitational potential energy to enable the ejection of the common envelope. Without this extra energy, it would be more difficult to eject the envelope around such a massive red giant and a $0.1 M_{\odot}$ M dwarf secondary, and the two might well merge (Sandquist et al. 2000).

8. SUBSEQUENT EVOLUTION

We consider the possible CV scenario for the subsequent evolution of 2M 1533+3759. If we assume gravitational radiation is the only acting mechanism for angular momentum loss and the secondary has not evolved on this timescale, the orbital period will decrease until the Roche lobe comes into contact with the secondary, initiating mass transfer and the beginning of the cataclysmic variable (CV) stage. The orbital period at contact, P_c , can be calculated using Kepler's law and the fact the ratio of the Roche lobe radius to the orbital separation is constant prior to contact: $P_c = P(a_c/a)^{1.5} = P(R_2/R_{L2})^{1.5}$, where a_c is the orbital separation at the beginning of contact, a is the current orbital separation, $R_2 = 0.152 R_{\odot}$ is the radius of the secondary (which is assumed not to change significantly), and $R_{L2} = 0.276 R_{\odot}$ is the current Roche lobe of the secondary Eggleton (1983).

The resulting P_c , 0.066 d (1.6 hr), will be above the minimum orbital period (1.27 hr) for a cataclysmic variable and below the period gap (Knigge 2006). If any additional mechanisms, such as magnetic braking, have a significant effect (see Sills et al. 2000), the timescale for Roche lobe contact would be reduced.

9. CONCLUSION

The sdB star 2M 1533+3759 is the seventh eclipsing sdB+dM binary discovered to date. Its orbital period of $0.16177042 \pm 0.00000001$ days is 29% longer than the 0.12505 day period of the next longest eclipsing sdB+dM, BUL-SC16 335. The amplitude of the reflection effect in 2M 1533+3759 is surprisingly strong, only about 0.05 mag weaker than the amplitude observed in HW Vir, in spite of the longer orbital period and the fact that the temperatures of the primary stars are similar.

2M 1533+3759 is the only new sdB binary among the eclipsing systems that were proposed to be sdB+dM by Kelley & Shaw (2007) on the basis of their narrow eclipse widths. This result is consistent with the 2MASS colors of other known reflection-effect sdB+dM systems, all of which have $J-H < 0$. 2M 1533+3759 and the archetypal HW Vir (Menzies & Marang 1986) are the only two binaries in Kelley & Shaw's (2007) Table 3 that have similarly blue IR colors, and the only two that contain sdB stars.

Spectroscopic parameters 2M 1533+3759 were derived by fitting Balmer and helium line profiles in high S/N spectra to a grid of zero-metallicity NLTE model atmospheres. The effective temperatures derived from low (9 Å) and medium (1.9 Å) resolution spectra exhibit clear variations with orbital phase. Phase variations are much less significant for the surface gravities, and completely negligible for the helium abundance fraction. Our adopted parameters for the sdB star, $T_{\text{eff}} = 29230 \pm 125$ K, $\log g = 5.58 \pm 0.03$, and $\log N(\text{He})/N(\text{H}) = -2.37 \pm 0.05$, were determined from medium-resolution spectra taken when the reflection effect was near minimum. The inferred rotational velocity has a negligible affect on the derivation of these parameters.

Light-curve modeling with the MORO code produced only one well-fitting solution consistent with a core helium burning primary. The system mass ratio, q (M_2/M_1), is 0.301 ± 0.014 and the inclination angle, i , is $86^{\circ}6 \pm 0.2$. The robustness and precision of these numbers are due to the high precision of the light curves and the fact that the system is eclipsing. Radial velocities for the sdB component were used to derive the velocity amplitude, $K_1 = 71.1 \pm 1.0$ km s⁻¹, leading to component masses of $M_1 = 0.376 \pm 0.055 M_{\odot}$ and $M_2 = 0.113 \pm 0.017 M_{\odot}$. The errors in the masses are dominated by the uncertainty in q . Since the mass ratio and inclination are even more uncertain in non-eclipsing systems, our inability to more tightly constrain the primary mass provides a strong illustration for why useful sdB masses from light-curve modeling can usually be obtained only from eclipsing binaries.

The orbital separation derived from the masses and the period is $a = 0.98 \pm 0.04 R_{\odot}$. The individual radii, $R_1 = 0.166 \pm 0.007 R_{\odot}$, and $R_2 = 0.152 \pm 0.005 R_{\odot}$, were then calculated from the relative radii, R_1/a and R_2/a , determined by the light-curve solution. Both radii are consistent with theoretical expectations, and the resulting sdB surface gravity, $\log g = 5.57 \pm 0.07$, is completely consistent with the adopted spectroscopic value above.

We constructed a synthetic line-blanketed spectrum to investigate potential systematic effects caused by our use of zero-metallicity NLTE atmospheres to derive the spectroscopic parameters. If 2M 1533+3759 had solar abundances of C, N, O, S, and Fe in its atmosphere, our assumption of zero metals would have overestimated the effective temperature by about 2000 K, and the surface gravity by almost 0.2 dex. Thus, the true T_{eff} and $\log g$ abundances would have been about 27,300 K and 5.40, respectively. The modeled light-curve solution at this lower temperature is only negligibly different from our original solution, and thus the resulting system parameters remain essentially unchanged. However, in this case, the calculated sdB surface gravity, $\log g = 5.57$, would be much less consistent with the expected value of 5.40. This suggests that the full correction to solar metallicities assumed above is not appropriate for 2M 1533+3759.

An important conclusion is that there is now significant observational evidence, from two completely independent techniques, asteroseismology (PG 0911+456) and modeling of eclipsing/reflection effect light curves (2M 1533+3759, and perhaps HS 2333+3927), for the existence of sdB stars with masses significantly lower than the canonical $0.48 \pm 0.02 M_{\odot}$.

2M 1533+3759 must have formed via the first common-envelope channel, since the companion is an M dwarf. With a probable sdB mass in the range 0.32–0.43 M_{\odot} , this star is expected to have evolved from a main-sequence A star with an initial mass >1.8 – $2.0 M_{\odot}$. The existence of such a binary might support recent theoretical predictions that sdB stars can be produced by such massive progenitors, including the assumption that the ionization energy of the red giant envelope contributes to the ejection of the common envelope (Han et al. 2002, 2003). If the primary mass of 2M 1533+3759 could be measured more precisely, or if the separation between the two components could be measured independently, this system ought to provide a very useful observational constraint for the upper limit to the main-sequence mass of an sdB progenitor.

If 2M 1533+3759 becomes a cataclysmic variable (CV) after orbital shrinkage due to gravitational radiation brings the Roche lobe into contact with the M dwarf secondary, its orbital period

of the CV at the onset of mass transfer will be 1.6 hr, below the CV period gap.

We acknowledge the invaluable assistance of the Steward mountain staff at the Catalina and Kitt Peak observatories. We are also in debt to Bill Peters for the excellent error treatment in his linearized least squares program, and to Roy Østensen for helping to resolve the question of NSVS 04818255. The authors thank the referee for thoughtful comments that helped to improve the original manuscript.

Note added in proof: After this paper was accepted, Dr. Prada-Moroni kindly pointed out their recent theoretical paper (Prada-Moroni & Straniero 2009) in which they follow in detail the evolution of low mass He-burning cores resulting from anomalously large mass loss during the red giant evolution of stars with initial main-sequence masses of $2.3 M_{\odot}$

REFERENCES

- Allard, F., Wesemael, F., Fontaine, G., Bergeron, P., & Lamontagne, R. 1994, *AJ*, **107**, 1565
- Althaus, L. G., Serenelli, A. M., & Benvenuto, O. G. 2001, *MNRAS*, **323**, 471
- Baraffe, I., & Chabrier, G. 1996, *ApJ*, **461**, L51
- Bayless, A. J., & Orosz, J. A. 2006, *ApJ*, **651**, 1155
- Binney, J., & Merrifield, M. 1998, *Galactic Astronomy* (Princeton Series in Astrophysics; Princeton, NJ: Princeton Univ. Press)
- Brown, T. M., Ferguson, H. C., Davidsen, A. F., & Dorman, B. 1997, *ApJ*, **482**, 685
- Castellani, M., & Castellani, V. 1993, *ApJ*, **407**, 649
- Charpinet, S., Fontaine, G., & Brassard, P. 2003, in NATO ASIB Proc. 105: White Dwarfs, ed. D. de Martino, R. Silvotti, J.-E. Solheim, & R. Kalytis (Dordrecht: Kluwer), 69
- Charpinet, S., Fontaine, G., Brassard, P., Billères, M., Green, E. M., & Chayer, P. 2005a, in ASP Conf. Ser. 334, 14th European Workshop on White Dwarfs, ed. D. Koester & S. Moehler (San Francisco, CA: ASP), 619
- Charpinet, S., Fontaine, G., Brassard, P., Chayer, P., Green, E. M., & Randall, S. K. 2007, *Commun. Asteroseismol.*, **150**, 241
- Charpinet, S., Fontaine, G., Brassard, P., Chayer, P., Rogers, F. J., Iglesias, C. A., & Dorman, B. 1997, *ApJ*, **483**, L123
- Charpinet, S., Fontaine, G., Brassard, P., & Dorman, B. 1996, *ApJ*, **471**, L103
- Charpinet, S., Fontaine, G., Brassard, P., Green, E. M., & Chayer, P. 2005b, *A&A*, **437**, 575
- Charpinet, S., van Grootel, V., Reese, D., Fontaine, G., Green, E. M., Brassard, P., & Chayer, P. 2008, *A&A*, **489**, 377
- Charpinet, S., et al. 2006, *A&A*, **459**, 565
- D'Cruz, N. L., Dorman, B., Rood, R. T., & O'Connell, R. W. 1996, *ApJ*, **466**, 359
- de Boer, K. S. 1982, *A&AS*, **50**, 247
- Diaz-Cordoves, J., Claret, A., & Gimenez, A. 1995, *A&AS*, **110**, 329
- Dorman, B., Rood, R. T., & O'Connell, R. W. 1993, *ApJ*, **419**, 596
- Drechsel, H., Haas, S., Lorenz, R., & Gayler, S. 1995, *A&A*, **294**, 723
- Drechsel, H., et al. 2001, *A&A*, **379**, 893
- Eggleton, P. P. 1983, *ApJ*, **268**, 368
- Fleig, J., Rauch, T., Werner, K., & Kruk, J. W. 2008, *A&A*, **492**, 565
- Fontaine, G., Brassard, P., Charpinet, S., Green, E. M., Chayer, P., Billères, M., & Randall, S. K. 2003, *ApJ*, **597**, 518
- Fontaine, G., Brassard, P., Charpinet, S., Green, E. M., Chayer, P., Randall, S. K., & van Grootel, V. 2008, in ASP Conf. Ser. 392, Hot Subdwarf Stars and Related Objects, ed. U. Heber, C. S. Jeffery, & R. Napiwotzki (San Francisco, CA: ASP), 231
- For, B.-Q., Edelmann, H., Green, E. M., Drechsel, H., Nesslinger, S., & Fontaine, G. 2008, in ASP Conf. Ser. 392, ed. U. Heber, C. S. Jeffery, & R. Napiwotzki (San Francisco, CA: ASP), 203
- Geier, S., Karl, C., Edelmann, H., Heber, U., & Napiwotzki, R. 2008, *Mem. Soc. Astron. Ital.*, **79**, 608
- Gray, R. O., & Corbally, C. 2009, *Stellar Spectral Classification* (Princeton, NJ: Princeton Univ. Press) (Appendix Tables A.1, A.6, and A.7)
- Green, E. M., Fontaine, G., Hyde, E. A., For, B.-Q., & Chayer, P. 2008, in ASP Conf. Ser. 392, Hot Subdwarf Stars and Related Objects, ed. U. Heber, C. S. Jeffery, & R. Napiwotzki (San Francisco, CA: ASP), 75
- Green, E. M., Liebert, J. W., & Saffer, R. A. 1997, in *The Third Conference on Faint Blue Stars*, ed. A. G. D. Philip, J. Liebert, R. Saffer, & D. S. Hayes (Schenectady, NY: L. Davis Press), 417
- Green, E. M., et al. 2003, *ApJ*, **583**, L31
- Green, E. M., et al. 2004, *Ap&SS*, **291**, 267
- Green, R. F., Schmidt, M., & Liebert, J. 1986, *ApJS*, **61**, 305
- Greggio, L., & Renzini, A. 1999, *Mem. Soc. Astron. Ital.*, **70**, 691
- Han, Z., Podsiadlowski, P., Maxted, P. F. L., & Marsh, T. R. 2003, *MNRAS*, **341**, 669
- Han, Z., Podsiadlowski, P., Maxted, P. F. L., Marsh, T. R., & Ivanova, N. 2002, *MNRAS*, **336**, 449
- Heber, U. 1986, *A&A*, **155**, 33
- Heber, U., et al. 2005, in ASP Conf. Ser. 334, 14th European Workshop on White Dwarfs, ed. D. Koester & S. Moehler (San Francisco, CA: ASP), 357
- Heber, U., et al. 2004, *A&A*, **420**, 251
- Hilditch, R. W., Harries, T. J., & Hill, G. 1996, *MNRAS*, **279**, 1380
- Hu, H., Nelemans, G., Østensen, R., Aerts, C., Vučković, M., & Groot, P. J. 2007, *A&A*, **473**, 569
- Kelley, N., & Shaw, J. S. 2007, *J. Southeastern Assoc. Res. Astron.*, **1**, 13
- Kilkenny, D., Koen, C., O'Donoghue, D., & Stobie, R. S. 1997, *MNRAS*, **285**, 640
- Kilkenny, D., O'Donoghue, D., Koen, C., Lynas-Gray, A. E., & van Wyk, F. 1998, *MNRAS*, **296**, 329
- Knigge, C. 2006, *MNRAS*, **373**, 484
- Koen, C. 2007, *MNRAS*, **377**, 1275
- Landsman, W., Bohlin, R. C., Neff, S. G., O'Connell, R. W., Roberts, M. S., Smith, A. M., & Stecher, T. P. 1998, *AJ*, **116**, 789
- Lee, J. W., Kim, S.-L., Kim, C.-H., Koch, R. H., Lee, C.-U., Kim, H.-I., & Park, J.-H. 2009, *AJ*, **137**, 3181
- Lisker, T., Heber, U., Napiwotzki, R., Christlieb, N., Han, Z., Homeier, D., & Reimers, D. 2005, *A&A*, **430**, 223
- Lucy, L. B. 1967, *Z. Astrophys.*, **65**, 89
- Maxted, P. F. L., Heber, U., Marsh, T. R., & North, R. C. 2001, *MNRAS*, **326**, 1391
- Maxted, P. F. L., Marsh, T. R., Heber, U., Morales-Rueda, L., North, R. C., & Lawson, W. A. 2002, *MNRAS*, **333**, 231
- Maxted, P. F. L., Morales-Rueda, L., & Marsh, T. R. 2004, *Ap&SS*, **291**, 307
- Meibom, S., et al. 2009, *AJ*, **137**, 5086
- Mengel, J. G., Norris, J., & Gross, P. G. 1976, *ApJ*, **204**, 488
- Menzies, J. W., & Marang, F. 1986, in *IAU Symposium 118, Instrumentation and Research Programmes for Small Telescopes*, ed. J. B. Hearnshaw & P. L. Cottrell (Dordrecht: Reidel), 305
- Moni Bidin, C., Catelan, M., Villanova, S., Piotto, G., Altmann, M., Momany, Y., & Moehler, S. 2008, in ASP Conf. Ser. 392, ed. U. Heber, C. S. Jeffery, & R. Napiwotzki (San Francisco, CA: ASP), 27
- Morales-Rueda, L., Maxted, P. F. L., Marsh, T. R., North, R. C., & Heber, U. 2003, *MNRAS*, **338**, 752
- Østensen, R. H., Oreiro, R., Hu, H., Drechsel, H., & Heber, U. 2008, in ASP Conf. Ser. 392, ed. U. Heber, C. S. Jeffery, & R. Napiwotzki (San Francisco, CA: ASP), 221
- Paczynski, B. 1980, *Acta Astron.*, **30**, 113
- Podsiadlowski, P., Han, Z., Lynas-Gray, A. E., & Brown, D. 2008, in ASP Conf. Ser. 392, Hot Subdwarf Stars and Related Objects, ed. U. Heber, C. S. Jeffery, & R. Napiwotzki (San Francisco, CA: ASP), 15
- Politano, M., Taam, R. E., van der Sluys, M., & Willems, B. 2008, *ApJ*, **687**, L99
- Polubek, G., Pigulski, A., Baran, A., & Udalski, A. 2007, in ASP Conf. Ser. 372, 15th European Workshop on White Dwarfs, ed. R. Napiwotzki & M. R. Burleigh (San Francisco, CA: ASP), 487
- Prada-Moroni, P. G., & Straniero, O. 2009, arXiv:0909.2742
- Randall, S. K., Fontaine, G., Charpinet, S., Lynas-Gray, A. E., Lopes, I. P., O'Toole, S. J., & Brassard, P. 2006, *ApJ*, **648**, 637
- Randall, S. K., et al. 2007, *A&A*, **476**, 1317
- Randall, S. K., van Grootel, V., Fontaine, G., Charpinet, S., & Brassard, P. 2009, *A&A*, in press, arXiv:0909.4404
- Rucinski, S. M. 2009, *MNRAS*, **395**, 2299
- Saffer, R. A., Bergeron, P., Koester, D., & Liebert, J. 1994, *ApJ*, **432**, 351
- Saffer, R. A., Green, E. M., & Bowers, T. 2001, in ASP Conf. Ser. 226, 12th European Workshop on White Dwarfs, ed. J. L. Provencal, H. L. Shipman, J. MacDonald, & S. Goodchild (San Francisco, CA: ASP), 408
- Sandquist, E. L., Taam, R. E., & Burkert, A. 2000, *ApJ*, **533**, 984
- Sills, A., Pinsonneault, M. H., & Terndrup, D. M. 2000, *ApJ*, **534**, 335
- Skrutskie, M. F., et al. 2006, *AJ*, **131**, 1163
- Swiegart, A. V., Greggio, L., & Renzini, A. 1989, *ApJS*, **69**, 911
- van Grootel, V., Charpinet, S., Fontaine, G., & Brassard, P. 2008a, *A&A*, **483**, 875

- van Grootel, V., Charpinet, S., Fontaine, G., Brassard, P., Green, E. M., Chayer, P., & Randall, S. K. 2008b, *A&A*, **488**, 685
- van Spaandonk, L., Fontaine, G., Brassard, P., & Aerts, C. 2008, *Commun. Asteroseismol.*, **156**, 35
- von Zeipel, H. 1924, *MNRAS*, **84**, 665
- Vučković, M., Aerts, C., Östensen, R., Nelemans, G., Hu, H., Jeffery, C. S., Dhillon, V. S., & Marsh, T. R. 2007, *A&A*, **471**, 605
- Vučković, M., Østensen, R., Bloemen, S., Decoster, I., & Aerts, C. 2008, in *ASP Conf. Ser. 392, Hot Subdwarf Stars and Related Objects*, ed. U. Heber, C. S. Jeffery, & R. Napiwotzki (San Francisco, CA: ASP), 199
- Wade, R. A., & Rucinski, S. M. 1985, *A&AS*, **60**, 471
- Wils, P., di Scala, G., & Otero, S. A. 2007, *IBVS*, 5800, 1
- Wilson, R. E., & Devinney, E. J. 1971, *ApJ*, **166**, 605
- Wood, J. H., & Saffer, R. 1999, *MNRAS*, **305**, 820
- Wood, J. H., Zhang, E.-H., & Robinson, E. L. 1993, *MNRAS*, **261**, 103
- Wozniak, P. R., et al. 2004, *VizieR Online Data Catalog*, **2287**, 0
- Yi, S., Demarque, P., & Oemler, A. J. 1997, *ApJ*, **486**, 201
- Yi, S., Lee, Y.-W., Woo, J.-H., Park, J.-H., Demarque, P., & Oemler, A. J. 1999, *ApJ*, **513**, 128
- Zahn, J.-P. 1977, *A&A*, **57**, 383